Looking at platinum carbonyl nanoclusters as superatoms

Jianyu Wei, Rémi Marchal, Didier Astruc, Samia Kahlal, Jean-François Halet, Jean-Yves Saillard

Looking at platinum carbonyl nanoclusters as *superatoms*

Jianyu Wei,[a,b] Rémi Marchal,[a] Didier Astruc,[b] Samia Kahlal,[a] Jean-François Halet,*[a,c] and Jean-Yves Saillard*[a]*

[a]Univ Rennes, CNRS, Institut des Sciences Chimiques de Rennes (ISCR) – UMR 6226, F 35000 Rennes, France. E-mail: samia.kahlal@univ-rennes1.fr, saillard@univ-rennes1.fr

[b]ISM, UMR CNRS 5255, University of Bordeaux, 351 Cours de la Libération, F-33405 Talence Cedex, France

[c]CNRS – Saint-Gobain – NIMS, IRL 3629, Laboratory for Innovative Key Materials and Structures (LINK), National Institute for Materials Science (NIMS), Tsukuba, 305-0044, Japan. E-mail: jean-francois.halet@univ-rennes1.fr.

Dedicated to the memory of Professor Larry F. Dahl, a pioneer and an immense contributor to ligated cluster chemistry.

Abstract: Although the chemistry of carbonyl-protected platinum nanoclusters is well established, their bonding mode remains poorly understood. In most of them, the average Pt oxidation state is zero or slightly negative, leading to the apparent average configuration $5d^{10}\,6s^{\varepsilon}$ (ε = 0 or very small) and the apparent conclusion that metal–metal bonding cannot arise from the completely filled 5d shell nor from the empty (or almost empty) 6s orbitals. However, DFT calculations show in fact that in these species the actual average configuration is $5d^{10-x}\,6s^{x}$, which provides to the whole cluster a significant total number of 6s electrons that ensures metal–metal bonding. This ("excited") average configuration is to be related to that of coinage metals in ligated group 11 nanoclusters ($nd^{10}\,(n+1)s^{x}$). Calculations show that metal–metal bonding in most of these platinum nanoclusters can be rationalized within the concepts of superatoms and supermolecules, in a similar way as for group 11 nanoclusters. The "excited" $5d^{10-x}\,6s^{x}$ configuration results from a level crossing between 5d combinations and 6s combinations, the former transferring their electrons to the latter. This level crossing, which does not exist in the bare Pt_n clusters, is induced by the ligand shell, the role of which being thus not innocent with respect to metal–metal bonding.

1. Introduction

The design and synthesis of atomically precise ligated nanoclusters is currently a very hot topic in nanoscience.[1-18] As part of this large family, that of gold nanoclusters is the most renowned one, but that of platinum nanoclusters, the exploration of which dates back to the late sixties,[19] is still widely investigated,[20-22] owing to their various properties and their use as models for size-controlled metallic platinum nanoparticles. Interestingly, whereas the structure, bonding and stability of ligated gold (and other group 11 metals) nanoclusters is nowadays well understood, thanks to the concept of *superatom*,[23-30] that of their group 10 homologues is not.[31-34]

The qualitative *superatom* model is based on the spherical *jellium* approximation,[35] which considers the electrons lying within a radial phenomenological potential supposed to describe the average electrostatic potential associated with the cluster atom nuclei. Replacing the dense spherical cloud of nuclei point-charges by such a smoothened radial potential allows describing the cluster electronic structure in terms of *superatomic* orbitals, resembling atomic orbitals (AOs), but extending over the whole cluster sphere.[23-30] Their shell ordering is largely independent from the cluster nature and spans as 1S < 1P < 1D < 2S < 1F, etc. As for atomic systems, closed-shell stability is achieved for specific ("*magic*") electron counts, *i.e.*, 2, 8, 18, 20, 34, etc. In the case of ligated nanoclusters of coinage metals (Cu, Ag, Au), the electrons that have to be considered in this count are those (and only those) coming from the valence (n + 1)s orbitals.[36,37] Indeed, in such species the mixed-valent metal atoms are in an average oxidation state comprised between 0 and +I, *i.e.,* in an nd^{10} (n + 1)s^{x} (0 < x < 1) configuration, thus with a fully occupied nd shell, implying that valence d electrons cannot significantly participate to metal–metal bonding. Thus, in first approximation, the *superatom* orbitals can be identified as the combinations of the (n + 1)s AOs. In the literature, the electrons they contain are called either *jellium*, *superatomic*, free, nearly free or delocalized electrons. In the followings, we choose to call them *free electrons* (*fe*) and their number *nfe*. This simple electron counting scheme works perfectly in the case of ligated group 11 metal clusters and indeed, most of them can be described as closed-shell *superatoms*[38-45] or closed-shell assemblies of *superatoms* (*supermolecules*).[33,46-54]

In the case of group 10 ligated nanoclusters, it turns out that the above methodology for counting electrons does not apply so staightforwardly. Thus, this

sizeable structural chemistry appears to stand outside the *superatom* concept and remains mostly unexplained. Indeed, in the majority of the structurally characterized Ni, Pd or Pt ligated nanoclusters, the average metal oxidation state is zero (valence nd^{10} $(n + 1)s^0$ metal configuration), or close to zero (nd^{10} $(n + 1)s^x, x \approx 0$), and one is driven to an apparent *superatom* electron count equal or close to zero. In other words, within the concept of *superatoms*, there are no (or not enough) electrons to ensure the metal-metal bonding within these clusters, which obviously contradicts the fact they exist.

We have recently shown that, in the case of ligated palladium nanoclusters, this mechanical electron counting is not appropriate. In fact, in such species, due to the peripheral ligand shell, some bonding combinations of the "empty" $(n + 1)s$ AOs are stabilized at sufficiently low energy for being occupied in the cluster, to the detriment of the same number of nd combinations of higher energy that are destabilized by the ligand lone pairs, and then get depopulated. In other words, the Pd average electron configuration in these species is nd^{10-x} $(n +1)s^x$. This is what happens in $[Pd_{13}(\mu_4\text{-}C_7H_7)_6]^{2+}$ (*nfe* = 2, $1S^2$ configuration)[55,56] and $Pd_{55}(PR_3)_{12}(\mu_3\text{-}CO)_{20}$ (*nfe* = 20, $1S^2$ $1P^6$ $1D^{10}$ $2S^2$ configuration) for instance.[57,58] In this paper, we move to platinum, which is also remarkable in its propensity to form high nuclearity carbonyl clusters, in particular the so-called family of "platinum browns",[31] which were mainly developed in the past in the group of Longoni and now that of Zacchini in Italy,[31,59-66] and to a lesser extent, in that of Dahl in the USA.[67,68] So, we explore a large series of this platinum nanocluster family and we demonstrate that, most of the time, it can also be rationalized within the concepts of *superatoms* and *supermolecules*. The specific and well-known branch of columnar $\{[Pt_3(CO)_6]_n\}^{2-}$ clusters[69,70] will not be considered here, as it has been fully rationalized in the past by Hoffmann and collaborators.[32,71] These high-nuclearity clusters resulting from different close-packed arrangements were tentatively rationalized via the so-called polyhedral skeletal electron pair theory (PSEPT) and its condensation principle extension[32,72,73] but as the cluster size increases, the energy differences between alternative arrangements become smaller and it is no longer possible to associate a particular cluster electron count with a specific cluster geometry.[32,73,74]

2. Computational details

Geometry optimizations were carried out at the density functional theory (DFT) level by using the ADF2018 code,[75] incorporating the relativistic Zeroth Order Regular Approximation (ZORA).[76] The Becke and Perdew (BP86) functional,[77,78] together with a triple-ζ basis set augmented with a polarization function (STO-TZP). Grimme's empirical DFT-D3 dispersion corrections[79] were included for taking into account of the van der Waals interactions. An energy convergence criterion of 5×10^{-5} Hartree and a radial convergence criterion of 5×10^{-3} Å were employed. The optimized structures were confirmed as genuine minima on their potential energy surface by analytical vibrational frequency calculations. Natural atomic orbital (NAO) populations[80] and Wiberg bond indices (WBI) were computed with the Gaussian 16 program[81] at the BP86/Def2-SVP[82] level using the ADF-optimized structures. For each cluster, *nfe* was obtained from the detailed analysis of its Kohn-Sham orbitals by detecting the occupied molecular orbitals of major Pt 6s character and identifying them as the cluster *superatomic* or *supermolecular* orbitals that contain the *fe'*s. Consistency with the nature of the lowest unoccupied combinations of large Pt 6s character, as well as the number of occupied and vacant combinations of major Pt 5d contribution was systematically controlled, allowing to safely treat the cases where 6s/5d mixing is significant. Unless specified in the figure captions, the orbitals are plotted with density isovalues of ± 0.01 $(e/bohr^3)^{1/2}$. For the sake of comparison, some of them are also plotted with a different isovalue in Figs. S2, S6 and S9).

3. Results and Discussions

3.1 Decorated 8-electron *superatoms* and related species

3.1.1. Experimentally characterized species

The compound $[NBu_4]_2[Pt_{13}(CO)_{12}\{Cd_5(\mu\text{-}Br)_5Br_2(dmf)_3\}_2]$ (dmf = dimethylformamide), isolated in 2011 by Zacchini and coworkers,[59,60] contains the complex anion $[Pt_{13}(CO)_{12}\{Cd_5(\mu\text{-}Br)_5Br_2(dmf)_3\}_2]^{2-}$ that can be described as a centred icosahedral $[Pt_{13}(CO)_{12}]^{8-}$ polyanion decorated with 10 Cd^{2+} cations, 14 Br^- anions, and 6 solvent molecules. The 12 carbonyl ligands being terminal, the idealized symmetry of $[Pt_{13}(CO)_{12}]^{8-}$ is I_h (Fig. 1 and Fig. S1, ESI). The cluster anion is isoelectronic with $[Au_{13}(PMe_2Ph)_{10}Cl_2]^{3+}$

synthezised a long time ago by Mingos and coworkers.[45] The latter is a *superatom* with *nfe* = 13 (Au_{13}) – 2 (Cl_2) – 3 (charge) = 8 and $1S^2$ $1P^6$ closed-shell configuration. It is easy to predict that the 8– charge of $[Pt_{13}(CO)_{12}]^{8-}$ provides the 8 electrons that will occupy the four 6s(Pt) bonding combinations that can be identified as the 1S and 1P *superatomic* orbitals. This is confirmed by analyzing the Kohn-Sham orbital diagram of $[Pt_{13}(CO)_{12}]^{8-}$ (Fig. 2 and Fig. S2, ESI), which shows that the 1S (a_g) and 1P (t_{1u}) orbitals lie at the bottom of the fully occupied 5d block, whereas the vacant 1D (h_g) level is situated above the π*(CO) combinations. Thus, in $[Pt_{13}(CO)_{12}]^{8-}$, the Pt average configuration is $5d^{10}$ $6s^{0.62}$ (0.62 = 8/13). The substantial computed HOMO-LUMO gap of $[Pt_{13}(CO)_{12}]^{8-}$ should be related to the complete filling of the 5d block. Whereas in this simple case the metal 5d AOs are not involved in the bonding, the radial 6p orbitals of the peripheral Pt atoms are to some extent. Indeed, these atoms are somewhat sp-hybridized. The outward-pointing hybrid (of 6p major character) is used for Pt–CO bonding, whereas the inward-pointing hybrid (of 6s major character) participates to the *superatomic* orbitals. Relevant computed data are given in Table S1 (ESI). Calculations on the fully decorated anion $[Pt_{13}(CO)_{12}\{Cd_5(\mu\text{-}Br)_5Br_2(dmf)_3\}_2]^{2-}$ provided similar results that found for the isolated cluster $[Pt_{13}(CO)_{12}]^{8-}$ (Table S2). One can notice the agreement with the experimental structure.[60] This result was expected owing to the electrostatic nature of the interaction between the various $[Pt_{13}(CO)_{12}]^{8-}$, Cd^{2+} and Br^- ions.

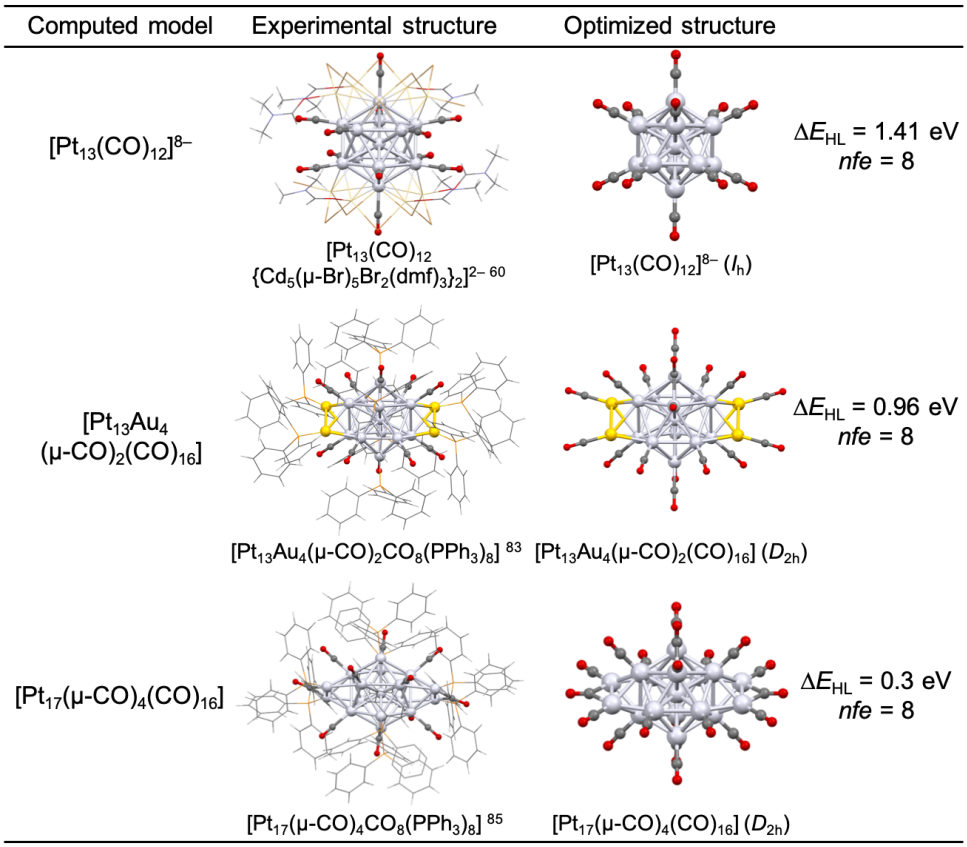

Figure 1 Optimized structures (right) of decorated icosahedral 8-electron *superatomic* models. EHL is the HOMO-LUMO gap. The corresponding experimental structures (left) are shown for comparison.

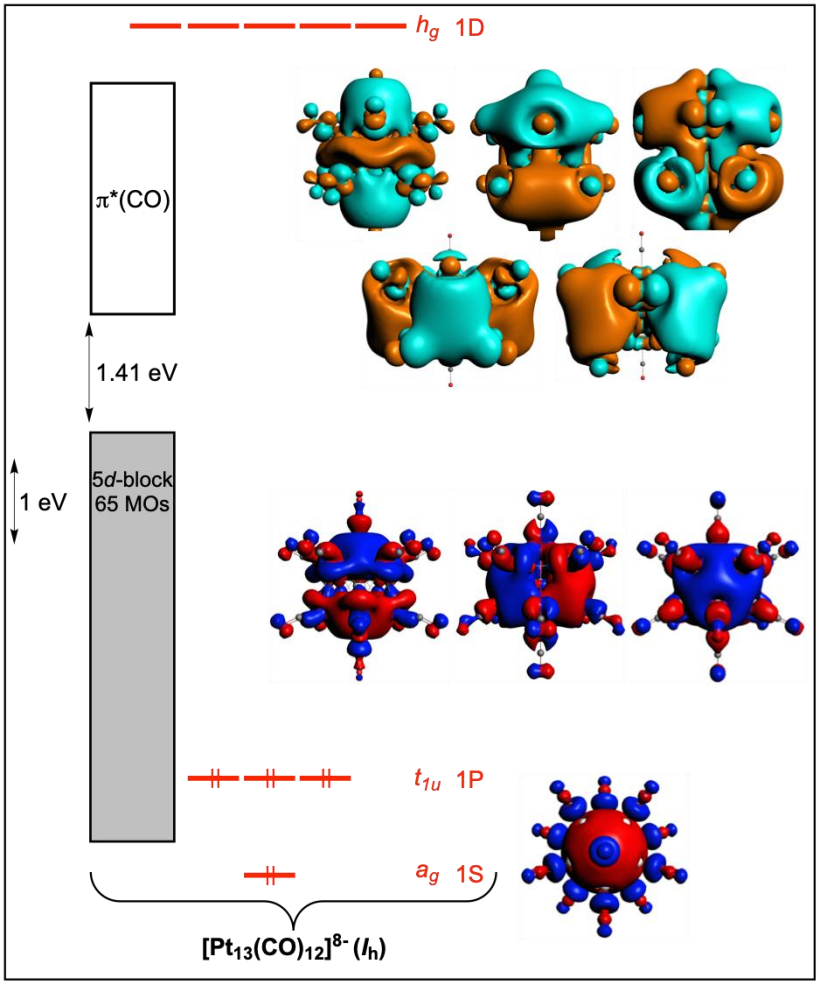

Figure 2 Kohn-Sham MO diagram of $[Pt_{13}(CO)_{12}]^{8-}$.

Two strongly related clusters that can also be described as made of a decorated $Pt_{13}L_{12}$ centred icosahedral unit, namely compounds $Pt_{13}[Au_2(PPh_3)_2]_2(\mu\text{-}CO)_2(CO)_8(PPh_3)_4$ [83] and $Pt_{13}[Pt_2(PR_3)_2(\mu\text{-}CO)]_2(\mu\text{-}CO)_2(CO)_8(PR_3)_4$ (R = Et, Ph),[84,85] have been also reported. Both clusters contain a central $Pt_{13}(CO)_8(PR_3)_4$ icosahedral unit, in which the 12 2-electron ligands are terminal, in a similar way as the CO ligands in $[Pt_{13}(CO)_{12}]^{8-}$. In $Pt_{13}[Au_2(PPh_3)_2]_2(\mu\text{-}CO)_2(CO)_8(PPh_3)_4$, the central unit is decorated with two supplementary CO ligands that bridge opposite edges of the icosahedron, and two bidentate $Ph_3PAu–AuPPh_3$ fragments that cap two opposite pairs of adjacent icosahedral faces (Fig. 1 and Fig. S1, ESI). The ideal symmetry of the latter is D_{2h}. $Pt_{13}[Pt_2(PR_3)_2(\mu\text{-}CO)]_2(\mu\text{-}CO)_2(CO)_8(PR_3)_4$ has the same structure and symmetry, except that the $Ph_3PAu–AuPPh_3$ fragment is now replaced by an isoelectronic $(PR_3)Pt–Pt(PR_3)(\mu\text{-}CO)$ fragment. Considering the $Ph_3PAu–AuPPh_3$ and $(PR_3)Pt–Pt(PR_3)(\mu\text{-}CO)$ fragments as 2-electron M_2L_n organometallic ligands, both $Pt_{13}[Au_2(PPh_3)_2]_2(\mu\text{-}CO)_2(CO)_8(PPh_3)_4$ and $Pt_{13}[Pt_2(PR_3)_2(\mu\text{-}CO)]_2(\mu_2\text{-}CO)_2(CO)_8(PR_3)_4$ can be viewed as Pt_{13} clusters

having a total of 162 cluster valence electrons (CVEs), *i.e.*, 13 x 10 (Pt) + 14 x 2 (L = CO, PR_3) + 2 x 2 (M_2L_n).[83] Not surprisingly, this is also the CVE count of $[Pt_{13}(CO)_{12}]^{8-}$ (13 x 10 + 12 x 2 + 8). This means that the two μ-CO and the two M_2L_n ligands have their 4 occupied frontier orbitals interacting with 4 combinations of the 5d block of the central $Pt_{13}(CO)_8(PR_3)_4$ icosahedral unit, thus making bonding and antibonding combinations, as sketched in Fig. 3 in the case of the model $Pt_{13}[Au_2(CO)_2]_2(\mu\text{-}CO)_2(CO)_{12}$. The computed Kohn-Sham orbital diagram of this model is given in Fig. S3 and that of $Pt_{13}[Pt_2(CO)_2(\mu\text{-}CO)]_2(\mu\text{-}CO)_2(CO)_{12}$ in Fig. S4 (ESI). DFT calculations on the simplified PH_3-substituted models $Pt_{13}[Au_2(PH_3)_2]_2(\mu\text{-}CO)_2(CO)_8(PH_3)_4$ and $Pt_{13}[Pt_2(PH_3)_2(\mu\text{-}CO)]_2(\mu\text{-}CO)_2(CO)_8(PH_3)_4$ are fully consistent with this qualitative description, as illustrated in Tables S3 and S4 (ESI). Thus, the occupied *superatomic* orbitals of the central $Pt_{13}L_{12}$ icosahedral unit are retained in $Pt_{13}[Au_2(PPh_3)_2]_2(\mu\text{-}CO)_2(CO)_8(PPh_3)_4$ and $Pt_{13}[Pt_2(PR_3)_2(\mu\text{-}CO)]_2(\mu\text{-}CO)_2(CO)_8(PR_3)_4$, which thus can also be viewed as 8-*fe superatoms*, in a similar way as $[Pt_{13}(CO)_{12}]^{8-}$ (*vide supra*). The involvement of some of the valence 5d orbitals in the bonding with "supplementary" ligands in these platinum *superatoms* is at variance with $[Pt_{13}(CO)_{12}]^{8-}$ and group 11 *superatoms*, in which all the valence *n*d combinations are fully non-bonding and occupied, *i.e.,* in which the ligands interact only with metal (*n* + 1)p or outward-pointing (*n* + 1)sp AOs. Since there are four 5d antibonding combinations that are unoccupied in their MO diagram, $Pt_{13}[Au_2(PPh_3)_2]_2(\mu\text{-}CO)_2(CO)_8(PPh_3)_4$ and $Pt_{13}[Pt_2(PR_3)_2(\mu\text{-}CO)]_2(\mu\text{-}CO)_2(CO)_8(PR_3)_4$ have lower HOMO-LUMO gaps than $[Pt_{13}(CO)_{12}]^{8-}$ (Table S1, ESI).

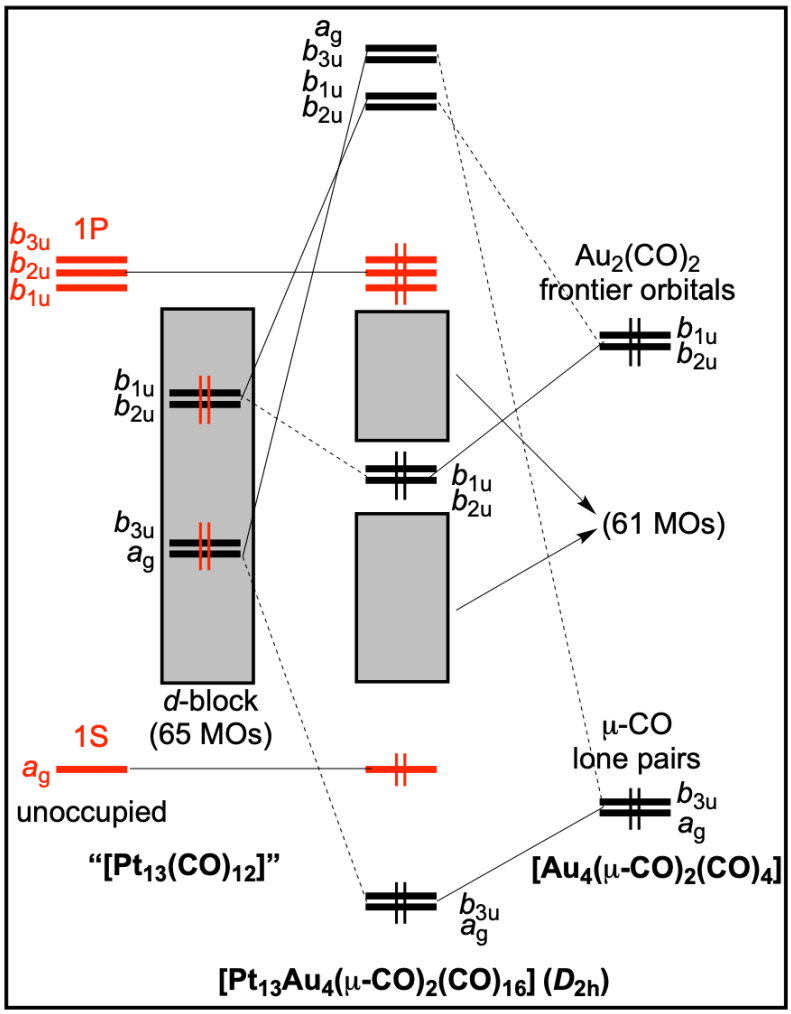

Figure 3 Qualitative MO interaction diagram between the icosahedral Pt13(CO)12 fragment and its two -CO and two Au2(CO)2 capping units in the [Pt13Au4(μ-CO)2(CO)16] model. Note that (i) the first fragment is formally in an excited state and (ii) the total number of occupied MOs (69) remains the same before and after interaction.

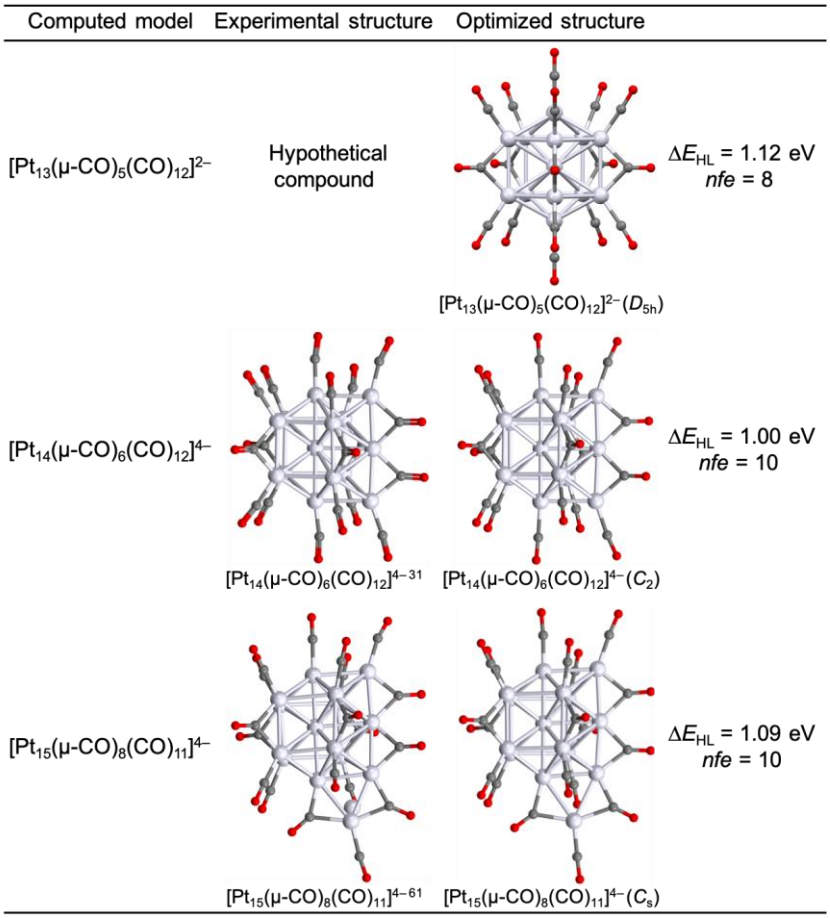

Figure 4 Optimized structures (right) of $[Pt_{13}(\mu\text{-}CO)_5(CO)_{12}]^{2-}$, $[Pt_{14}(\mu\text{-}CO)_6(CO)_{12}]^{4-}$ and $[Pt_{15}(\mu\text{-}CO)_8(CO)_{11}]^{4-}$. ΔE_{HL} is the HOMO-LUMO gap. The corresponding experimental structures (left) are shown for comparison where available.

3.1.2. The hypothetical D_{5h} $[Pt_{13}(\mu\text{-}CO)_5(CO)_{12}]^{2-}$ model: The versatile role of "additional" bridging ligands

As discussed just above, the $Pt_{13}[Au_2(PPh_3)_2]_2(\mu\text{-}CO)_2(CO)_8(PPh_3)_4$ and $Pt_{13}[Pt_2(PR_3)_2(\mu\text{-}CO)]_2(\mu\text{-}CO)_2(CO)_8(PR_3)_4$ clusters can be described as made of an icosahedral $Pt_{13}(CO)_{12}$ central unit, decorated by four "additional" ligands, namely two μ-CO and two η^6:μ_3, μ_3-M_2L_n units. The four orbitals containing the four electron pairs provided by these four ligands interact with 5d(Pt) combinations in such a way that a significant HOMO-LUMO gap is created for the magic 8-*fe* count (see Fig. 4, Fig. S5 (ESI) and related discussion above). As regard to "additional" carbonyls, one could expect that the lone-pair of any of them would destabilize one 5d(Pt) combination above the HOMO, as in regular "Wade-Mingos" organometallic clusters.[32] Therefore, assuming such one-to-one orbital interaction scheme, the number of destabilized (thus depopulated) 5d(Pt) combinations should be equal to the number of "additional"

carbonyls. It turns out that this is not always the case. It can happen that the number of 5d(Pt) combinations destabilized above the HOMO is lower than the number of "additional" carbonyls. This is exemplified by the hypothetical D_{5h} $[Pt_{13}(\mu\text{-}CO)_5(CO)_{12}]^{2-}$ model, which exhibits a bicapped centred pentagonal prismatic Pt_{13} core, a structure somewhat less compact and spherical than the icosahedron, but which offers five edges to be easy bridged by "additional" carbonyls (Fig. 4, top). Whereas the destabilization of five 5d(Pt) combinations (of $a'_1 + e'_1 + e'_2$ symmetry) by the five μ-CO lone-pair combinations is expected, only three of them (of $a'_1 + e'_2$ symmetry) actually are. This situation is sketched on the left side of Fig. 5 (see also Fig. S6, ESI). The large computed HOMO-LUMO gap (1.12 eV) undoubtedly indicates stability. This dianion is likely to be isolated as its salt in the future. On the other hand, the corresponding dication was not found to be stable. Although not very spherical, $[Pt_{13}(\mu\text{-}CO)_5(CO)_{12}]^{2-}$ has occupied pseudo-spherical *superatomic* orbitals of 1S and 1P nature (see Fig. 5 and Fig. S6, ESI), making it an 8-*fe superatom*.

3.1.3. Non-spherical clusters related to the D_{5h} $[Pt_{13}(\mu\text{-}CO)_5(CO)_{12}]^{2-}$ model: $[Pt_{14}(\mu\text{-}CO)_6(CO)_{12}]^{4-}$ and $[Pt_{15}(\mu\text{-}CO)_8(CO)_{11}]^{4-}$

The two relatively small and non-spherical clusters $[Pt_{14}(\mu\text{-}CO)_6(CO)_{12}]^{4-}$ and $[Pt_{15}(\mu\text{-}CO)_8(CO)_{11}]^{4-}$ experimentally reported[31,61] (Fig. 4 and Fig. S5, ESI) are both structurally related to the hypothetical D_{5h} $[Pt_{13}(\mu\text{-}CO)_5(CO)_{12}]^{2-}$ model discussed just above. Going from the latter to $[Pt_{14}(\mu\text{-}CO)_6(CO)_{12}]^{4-}$ corresponds formally to the insertion of a supplementary Pt atom in one of the edges connecting the two pentagons, together with the addition of a μ-CO ligand attached to this Pt atom. Note also the cluster charge variation. The idealized geometry of $[Pt_{14}(\mu\text{-}CO)_6(CO)_{12}]^{4-}$ is of C_{2v} symmetry, but the optimized structure was found slightly distorted to C_2. Analysis of its electronic structure indicates that the cluster has one more occupied 6s(Pt) combination than $[Pt_{13}(\mu\text{-}CO)_5(CO)_{12}]^{2-}$, which is located around the "additional" Pt atom (Fig. 4). The number of unoccupied 5d(Pt) combinations is unchanged, so the two "additional" electrons are used for filling this supplementary 6s(Pt) combination (Fig. 5) leading to a count of 10 *fe's* and the $1S^2\ 1P^6\ 2S^2$ closed-shell configuration. Going now from $[Pt_{14}(\mu\text{-}CO)_6(CO)_{12}]^{4-}$ to $[Pt_{15}(\mu\text{-}CO)_8(CO)_{11}]^{4-}$ consists in the formal insertion of a linear Pt(CO) unit on a Pt–Pt edge (Fig. 4). Such a Pt(CO) unit formally donates 2 electrons to the Pt–Pt edge it bridges and receives two electrons from its carbonyl neighbors, which move

from terminal to bridging upon Pt(CO) insertion. Thus, the number of cluster electrons does not change upon insertion of this Pt(CO) ligand. It follows that the electronic structures of $[Pt_{14}(\mu\text{-}CO)_6(CO)_{12}]^{4-}$ and $[Pt_{15}(\mu\text{-}CO)_8(CO)_{11}]^{4-}$ are basically the same, corresponding to non-spherical species with *nfe* = 10 (Fig. 5). Their occupied 6s(Pt) combination are plotted in Fig. S7 (ESI). Selected computed data are provided in Table S5 (ESI).

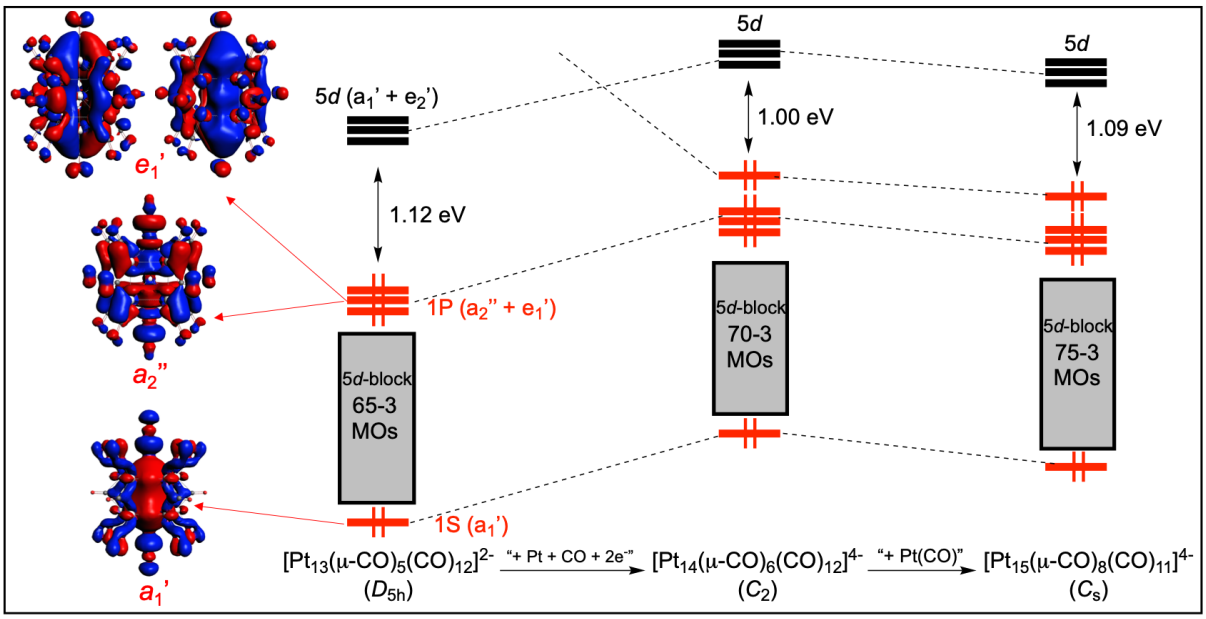

Figure 5 Kohn-Sham orbital diagram of $[Pt_{13}(\mu\text{-}CO)_5(CO)_{12}]^{2-}$ (left), $[Pt_{14}(\mu\text{-}CO)_6(CO)_{12}]^{4-}$ (middle) and $[Pt_{15}(\mu\text{-}CO)_8(CO)_{11}]^{4-}$ (right).

3.2 Assemblies of individual *superatoms*

3.2.1. Experimentally characterized species

Non-spherical metal group 11 nanoclusters, the structure of which can be described as resulting from the assembly of several pseudo-spherical individual units (most often icosahedral) are becoming quite common.[33,51,52,86-90] In such assemblies, the icosahedral units share either a vertex, a triangular face or are interpenetrated in such a way they share a pentagonal face and its two capping atoms. Such assemblies of individual *superatomic* units can be viewed as "*supermolecules*", with *supermolecular* orbitals looking like molecular orbitals, and electron counts related to that of simple main-group molecules, depending on their fusion extent, in the same way as molecule electron counts depend on bond orders (BOs).[52,91,92] Concerning group 11 nanoclusters made of two fused centred icosahedra, vertex-sharing systems have favored *superatomic* closed-shell electron counts of 16 or 14, *i.e.*, equivalent to Ne_2 (BO = 0) or F_2 (BO = 1), respectively.[90,93] Face-sharing icosahedra can also have a

favored count of 14[93] whereas interpenetrated icosahedra can display a favored count of 10, *i.e.*, equivalent to N_2 (BO = 3).[94]

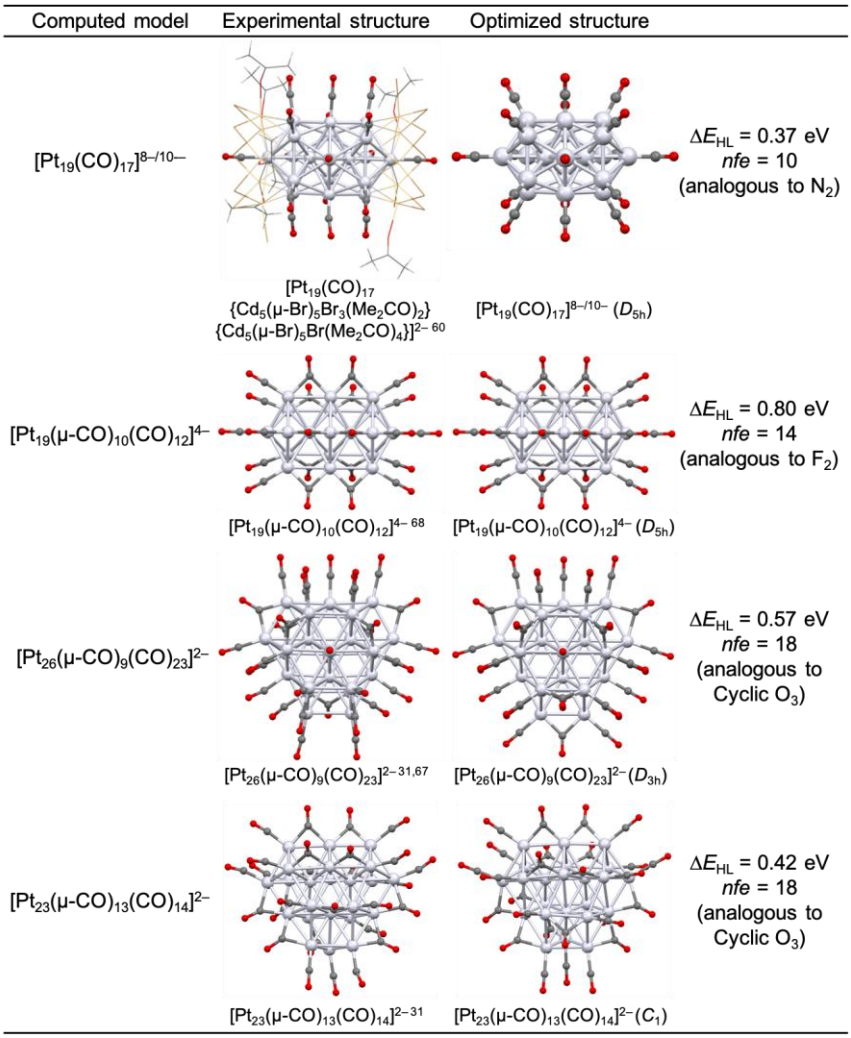

Figure 6 Optimized structures (right) of experimentally characterized clusters that can be viewed as linear assemblies of individual *superatoms*. ΔE_{HL} is the HOMO-LUMO gap. The corresponding experimental structures (left) are shown for comparison.

It turns out that a platinum cluster made of two interpenetrated icosahedra, namely $[Pt_{19}(CO)_{17}]^{8-}$ (Fig. 6 and Fig. S8, ESI), was shown to exist as a decorated polyanion in the solid state compound $[PPh_3Me]_2[Pt_{19}(CO)_{17}\{Cd_5(\mu\text{-}Br)_5Br_3(Me_2CO)_2\}\{Cd_5(\mu\text{-}Br)_5Br(Me_2CO)_4\}]$ isolated some years ago by Zacchini and coworkers.[59,60] In this cluster of ideal D_{5h} symmetry, the 17 CO ligands are terminally bonded to the 17 peripheral Pt atoms. Assuming an average Pt $5d^{10}$ $6s^{0.42}$ (0.42 = 8/19) configuration ends up with the apparent *superatomic* count *nfe* = 8. DFT calculations indicated that in fact this number is 10, occupying five *supermolecular* orbitals of large 6s(Pt) character having similar nodal properties as the $1\sigma_g$, $1\sigma_u$, $1\pi_u$ and $2\sigma_g$ molecular orbitals of N_2. Vacant orbitals analogues to the $1\pi_g^*$ and $2\sigma_u^*$ combinations can be

found at higher energies. Moreover, $[Pt_{19}(CO)_{17}]^{8-}$ is found to have a triplet ground-state, with a half-filled *e'₁* HOMO of large 5d(Pt) character. With two more electrons, $[Pt_{19}(CO)_{17}]^{10-}$ has a closed-shell configuration, with a significant, although moderate, HOMO-LUMO gap (0.37 eV). Its Kohn-Sham molecular diagram is shown in Fig. 7 (see also Fig. S9, ESI). Thus, in spite of their different charges, both $[Pt_{19}(CO)_{17}]^{8-}$ and $[Pt_{19}(CO)_{17}]^{10-}$ are 10-*nfe supermolecules*. Indeed, they differ from their number of 5d electrons. In $[Pt_{19}(CO)_{17}]^{10-}$ these ten electrons are coming from the overall 10– charge of the cluster, and occupy low-lying *supermolecular* orbitals. With two less electrons, $[Pt_{19}(CO)_{17}]^{8-}$turns to have a half-occupied 5d-based *e'₁* HOMO, making $[Pt_{19}(CO)_{17}]^{8-}$ an unsaturated triplet. The thermodynamical stability of $[Pt_{19}(CO)_{17}]^{8-}$ is to be related to the localization of its spin density on its Pt_{19} kernel and its protection by the ligand shell (Fig. S10, ESI), as well as its ionic decoration in the fully decorated $[Pt_{19}(CO)_{17}\{Cd_5(\mu\text{-}Br)_5Br_3(Me_2CO)_2\}\{Cd_5(\mu\text{-}Br)_5Br(Me_2CO)_4\}]^{4-}$ (Fig. S11, ESI). The electronic situation of $[Pt_{19}(CO)_{17}]^{8-}$ is reminiscent of that of the icosahedral $Pd_{55}(PR_3)_{12}(\mu_3\text{-}CO)_{20}$ *superatom*, which also has a triplet ground state configuration with a "magic" *nfe* count of 20 (*superatomic* $1S^2\,1P^6\,1D^{10}\,2S^2$ configuration).[58] The calculated metrical data of $[Pt_{19}(CO)_{17}]^{8-}$ are in good agreement with their experimental counterparts,[60] as well as that of the fully decorated $[Pt_{19}(CO)_{17}\{Cd_5(\mu\text{-}Br)_5Br_3(Me_2CO)_2\}\{Cd_5(\mu\text{-}Br)_5Br(Me_2CO)_4\}]^{2-}$ (Tables S6 and S7, ESI).

The metal core of $[Pt_{19}(\mu\text{-}CO)_{10}(CO)_{12}]^{4-}$ [68] is related to that of $[Pt_{19}(CO)_{17}]^{8-}$ in that it derives from the latter through a 36° rotation of its middle Pt_5 ring (Fig. 6 and Fig. S8, ESI). In other words, whereas the cluster core of $[Pt_{19}(CO)_{17}]^{8-}$ results from the interpenetration of two centred icosahedra, that of $[Pt_{19}(\mu\text{-}CO)_{10}(CO)_{12}]^{4-}$ is made of two interpenetrated bi-capped centred pentagonal prisms. This moderate rotational change slightly lowers the cluster compactness, and makes additional space for allowing 10 additional μ-CO ligands. The whole cluster symmetry is D_{5h} (Table S8). Analysis of its Kohn-Sham orbital diagram (Fig. 8) allows identifying 14 occupied *supermolecular* orbitals, making $[Pt_{19}(\mu\text{-}CO)_{10}(CO)_{12}]^{4-}$ a closed-shell *supermolecule* with *nfe* = 14, analogous to F_2 with the $1\sigma_g^2\,1\sigma_u^2\,\pi_u^4\,2\sigma_g^2\,\pi_g^4\,2\sigma_u^0$ electron configuration. Considering the tetra-anionic charge of the cluster, a level crossing occurs between five 6s(Pt) and five 5d(Pt) combinations, the latter transferring their 10 electrons into the former. Thus, in this particular case, the number of destabilized 5d(Pt) combinations is equal to that of the "additional" CO ligands (5 = 22 (total of COs) – 17 (total of surface Pt atoms)).

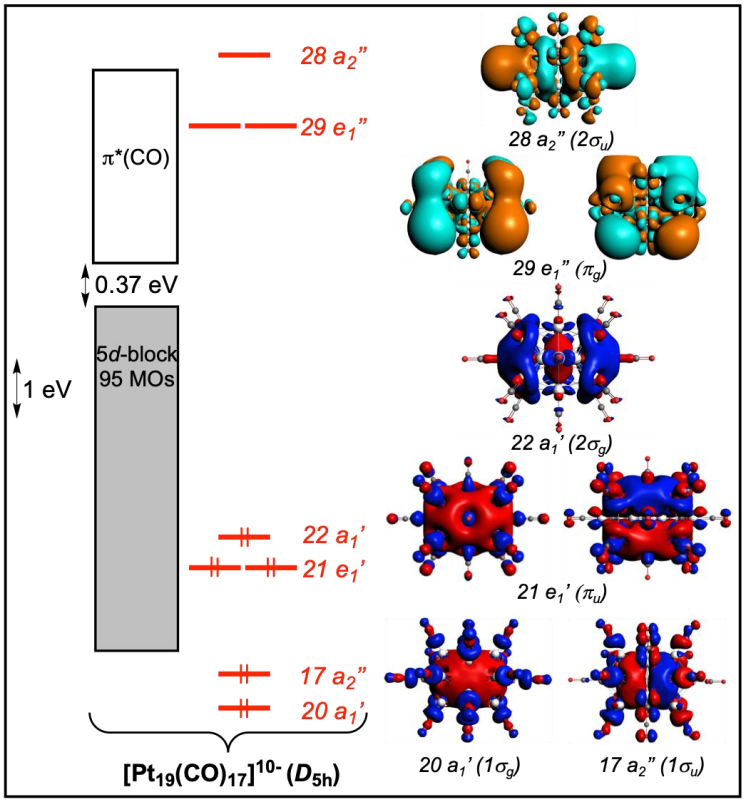

Figure 7 Kohn-Sham orbital diagram of $[Pt_{19}(CO)_{17}]^{10-}$. The *supermolecular* orbitals plotted on the right side are reminiscent of the valence orbitals of N_2.

It is noteworthy that $[Pt_{19}(CO)_{17}]^{8-/10-}$ and $[Pt_{19}(\mu\text{-}CO)_{10}(CO)_{12}]^{4-}$ differ by their number of *supermolecular* electrons (*nfe* = 10 and 14, respectively). The total cluster valence electron (CVE) counts (232/234 and 238, respectively) follow the same trend, and is consistent with the fact that the metallic core of the more electron-rich prismatic cluster $[Pt_{19}(\mu\text{-}CO)_{10}(CO)_{12}]^{4-}$ is less compact than that of the antiprismatic cluster $[Pt_{19}(CO)_{17}]^{8-/10-}$.

Cyclic assemblies of platinum *superatoms* can also exist as exemplified by $[Pt_{26}(\mu\text{-}CO)_9(CO)_{23}]^{2-}$.[31,67] This cluster possesses a non-pseudo-spherical core of ideal D_{3h} symmetry that can be described as a piece of *hcp* metal made of the *ABA* stacking of *hc* layers of 7, 12 and 7 atoms, respectively (Fig. 6 and Fig. S8, ESI).[31,67] It can be also viewed as a flattened (oblate) 2-shell $Pt_3@Pt_{23}$ system. Alternatively, one can look at it as made of three interpenetrated centred anti-cuboctahedra, their three centers constituting the encapsulated triangle of the $Pt_3@Pt_{23}$ system. Six vertices are shared between two centred anti-cuboctahedra and four are common to the three of them. There is a terminal carbonyl on each of the outer metals and 9 additional bridging ones. Its computed HOMO-LUMO gap (0.57 eV) is consistent with closed-shell stability. Examination of its electronic structure (Fig.

S12 and Table S9, ESI) indicates that it is an 18-electron species, which is best described as a *supermolecule* made of the triangular assembly of three interpenetrating centred anti-cuboctahedral *superatoms*. It is equivalent to the hypothetical triangular isomer of ozone (18 valence electrons),[95-99] as exemplified by the correspondence between the *supermolecular* orbitals of $[Pt_{26}(\mu\text{-}CO)_9(CO)_{23}]^{2-}$ and the molecular orbitals of cyclic O_3. In this particular case, the nine "additional" CO ligands induce the level crossing of only eight 5d(Pt) with eight 6s(Pt) combinations, inducing the transfer of 16 electrons into the latter. The cluster anionic charge provides 2 supplementary electrons.

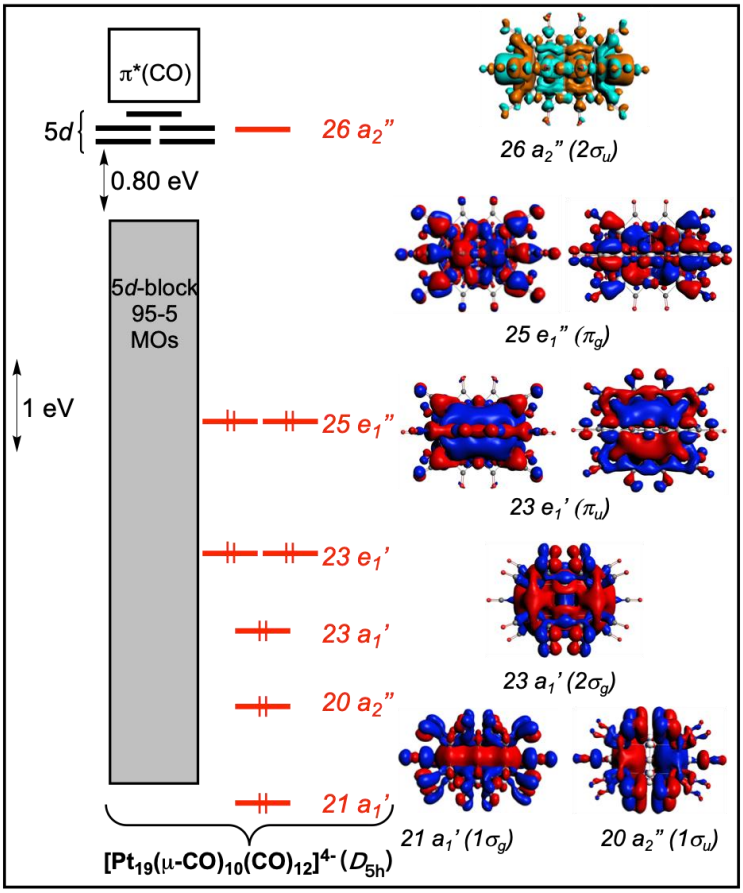

Figure 8 Kohn-Sham orbital diagram of $[Pt_{19}(\mu\text{-}CO)_{10}(CO)_{12}]^{4-}$. The *supermolecular* orbitals plotted on the right side are reminiscent of the valence orbitals of F_2.

The metal core arrangement of $[Pt_{23}(\mu\text{-}CO)_{13}(CO)_{14}]^{2-}$ [31] can be described as a defect structure of that of $[Pt_{26}(\mu\text{-}CO)_9(CO)_{23}]^{2-}$ with *ABA* stacking of 5, 12 and 6 atoms, respectively ($Pt_3@Pt_{20}$ (Fig. 6 and Fig. S8, ESI). Nevertheless, in this molecule of low symmetry it is still possible to identify three 11-vertex incomplete (and distorted) anti-cuboctahedra interpenetrating each other. Its computed HOMO-LUMO gap of 0.45 eV (Table S10, ESI) and

its electronic structure are also consistent with a description of an 18-electron *supermolecule* equivalent to cyclic O_3.

3.2.2. Hypothetical models

Starting from two interpenetrating centred icosahedra like in $[Pt_{19}(CO)_{17}]^{8-}$ (see above) it is possible to build linear oligomeric structures made of the interpenetration of several centred icosahedra. With three of them and assuming terminal ligands on every peripheral metal, the $Pt_{25}(CO)_{22}$ structure of D_{5d} symmetry was designed (Fig. 9 and Fig. S13, ESI). Calculations found the corresponding $[Pt_{25}(CO)_{22}]^{12-}$ anion to be a thermodynamically stable closed-shell species with a significant HOMO-LUMO gap of 0.63 eV, (Table S11, ESI). Examination of its electronic structure (Fig. S14, ESI) indicates that this 3-*superatom* model species is a 16-electron *supermolecule*. Within the $D_{\infty h}$ pseudosymmetry, the 16 electrons occupy *supermolecular* orbitals of σ_g (two), σ_u (two), π_g (one) and π_u (one) nature, thus making cluster $[Pt_{25}(CO)_{22}]^{12-}$ equivalent to CO_2. The 16 electrons are provided in part by the anionic charge and in part by the transfer of 4 electrons from two 5d-type combinations into two 6s combinations.

Computed model	Optimized structure	
$[Pt_{25}(CO)_{22}]^{12-}$ (D_{5d})	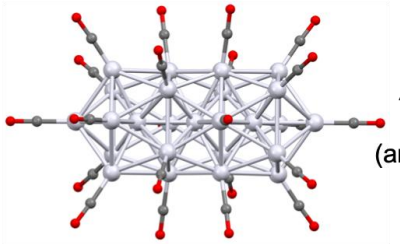	ΔE_{HL} = 0.63 eV *nfe* = 16 (analogous to CO_2)
$[Pt_{23}(CO)_{20}]^{12-}$ (D_{3h})	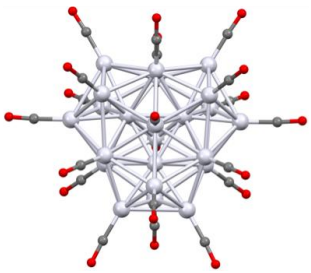	ΔE_{HL} = 0.57 eV *nfe* = 20
$[Pt_{23}(CO)_{21}]^{10-}$ (D_{3h})	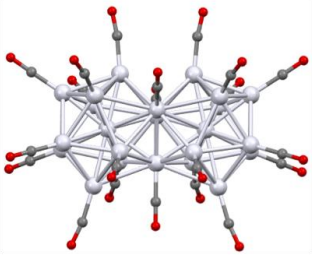	ΔE_{HL} = 0.51 eV *nfe* = 14 (analogous to F_2)

Figure 9 Optimized structures of linear assemblies of individual icosahedral *superatoms* (hypothetical models). ΔE_{HL} is the HOMO-LUMO gap.

One can also build an equilateral assembly of three interpenetrating icosahedra, resulting in a D_{3h} $Pt_3@Pt_{20}$ core. Assuming the existence of 20 terminal ligands, the structure is found thermodynamically stable for the unique 20-*nfe* count, *i.e.*, $[Pt_{23}(CO)_{20}]^{12-}$ (Fig. 9 and Fig. S13, ESI), with a HOMO-LUMO gap of 0.57 eV (Fig. S15 and Table S12, ESI). This unexpected electron count was also previously predicted for related Ag-rich structures.[52]

It is of course possible to imagine various types of linear assemblies made of several fused *superatomic* units. For example, assuming the Pt_{23} core made of two face-sharing centred icosahedra, with terminal carbonyls on each of the 21 peripheral metal atoms (Fig. 9 and Fig. S13, ESI), leads to the D_{3h} $Pt_{23}(CO)_{21}$ framework, for which a closed-shell ground state was found for a charge of 10–. Examination of its electronic structure (Fig. S16 and Table S13, ESI) leads to describe it as a species with an *nfe* = 14, equivalent of F_2 (two vacant 5d combinations).

Of course, one can argue that such highly charged hypothetical anions are unlikely to be isolated. One may however remark that real anionic clusters, such as $[Pt_{13}(CO)_{12}]^{8-}$, $[Pt_{19}(CO)_{17}]^{8-}$ and $[Pt_{19}(\mu\text{-}CO)_{10}(CO)_{12}]^{4-}$ for instance, exist (see above), being stabilized by a more or less complex cationic decorating shell.[59,60] Moreover, the presence of additional bridging ligands such as in $Pt_{13}[Au_2(PPh_3)_2]_2(\mu\text{-}CO)_2(CO)_8(PPh_3)_4$ and $Pt_{13}[Pt_2(PR_3)_2(\mu\text{-}CO)]_2(\mu\text{-}CO)_2(CO)_8(PR_3)_4$ [83-85] (and not considered in our models) could also help reducing the cluster charge by bringing supplementary electrons to the structure (see above). It seems thus likely that new Pt (or Pd) *supermolecular* clusters made of the linear (or cyclic) assembly of fused centred icosahedra (and/or centred bicapped pentagonal prisms) will be characterized in the future.

3.3 Other clusters with 3D architectures

3.3.1 Pseudo-spherical species

Any pseudo-spherical species should be described as a regular *superatom*, providing its metal core is sufficiently compact. This is the case of $[Pt_{38}(\mu\text{-}CO)_{12}(CO)_{32}]^{2-}$,[63,67] which exhibits an O_h metal core that is a piece of *fcc* metal resulting from the ABBA stacking of *hc* layers of 7, 12, 12 and 7 atoms, respectively (Fig. 10 and Fig. S17, ESI).

Alternatively, it can be viewed as made of two concentric O_h polyhedra ($Pt_6@Pt_{32}$). This metal core is passivated by a shell of 44 CO ligands, reducing the ideal symmetry to D_{2d}. Examination of the cluster electronic structure (Fig. S18, ESI) indicates that it is a *superatom* with $1S^2\ 1P^6\ 1D^{10}$ configuration (*nfe* = 18). These 18 electrons located in MOs of large 6s(Pt) character are originating in part from the cluster anionic charge and in the other part from the destabilization of eight 5d combinations, which in turn get depopulated. This 8-level block lies 0.45 eV above the HOMO (Fig. S18 and Table S14, ESI). The structure of the related species $[Pt_{36}(\mu\text{-}CO)_{18}(CO)_{26}]^{2-}$ (Fig. 10 and Fig. S17, ESI)[31] can be conceptually derived from that of $[Pt_{38}(\mu\text{-}CO)_{12}(CO)_{32}]^{2-}$ by the removal of two Pt atoms from one of the 7-atom layer and a reorganization of the ligand shell. Its optimized geometry (Table S15, ESI) is of C_{2v} symmetry, and its HOMO-LUMO gap is rather small (0.24 eV). Nevertheless, it is still possible to identify in its orbital spectrum 9 occupied levels of large 6s(Pt) character that attributes to $[Pt_{36}(\mu\text{-}CO)_{18}(CO)_{26}]^{2-}$ the character of 18-electron *superatom* (Fig. S19, ESI).

3.3.2 Non-pseudo-spherical species

Superatoms can move away from sphericity through oblate (flattening) or prolate (elongating) deformations that can be described as Jahn-Teller distortions associated with degeneracy splitting of *superatomic* electron shells, thus inducing electron counts that deviate from the *magic* numbers. This is the case of the isoelectronic clusters $[Pt_{19}(\mu_3\text{-}CO)_3(\mu\text{-}CO)_3(CO)_{18}(\mu_4\text{-}AuPPh_3)_3]^-$ and $[Pt_{19}(\mu_3\text{-}CO)(\mu\text{-}CO)_5(CO)_{18}\{\mu_4\text{-}Au_2(PPh_3)_2\}_2]$,[100] which can be described as prolate species. They exhibit similar Pt_{19} core made of the *fcc ABCA* packing of *hc* layers of 3, 7, 6 and 3 atoms (Fig. 10 and Fig. S17, ESI). The computed HOMO-LUMO gaps of their PH_3-substituted models, respectively 1.06 eV and 0.94 eV, are large (Table S16 and S17, ESI). In the D_{3h} pseudo-symmetry of their metal core the five-fold 1D level is split into 3-below-2 *superatomic* orbitals, generating the $1S^2\ 1P^6\ 1D^6$ configuration (14-*fe* species).

In the same vein, the unique large platinum cluster with a *bcc* metal core, namely $[Pt_{40}(\mu\text{-}CO)_{16}(CO)_{24}]^{6-}$ (Fig. 10, Fig. S17 and Table S18, ESI),[62] has an elongated shape that can be viewed as a distorted sphere. It can be associated with an *nfe* count of 28 with the $1S^2\ 1P^6\ 1D^{10}\ 2S^2\ 1F^8$ configuration resulting from a degeneracy splitting of the 1F shell in D_{2h} symmetry, although the small computed HOMO-LUMO gap leaves some doubts about this cluster description.

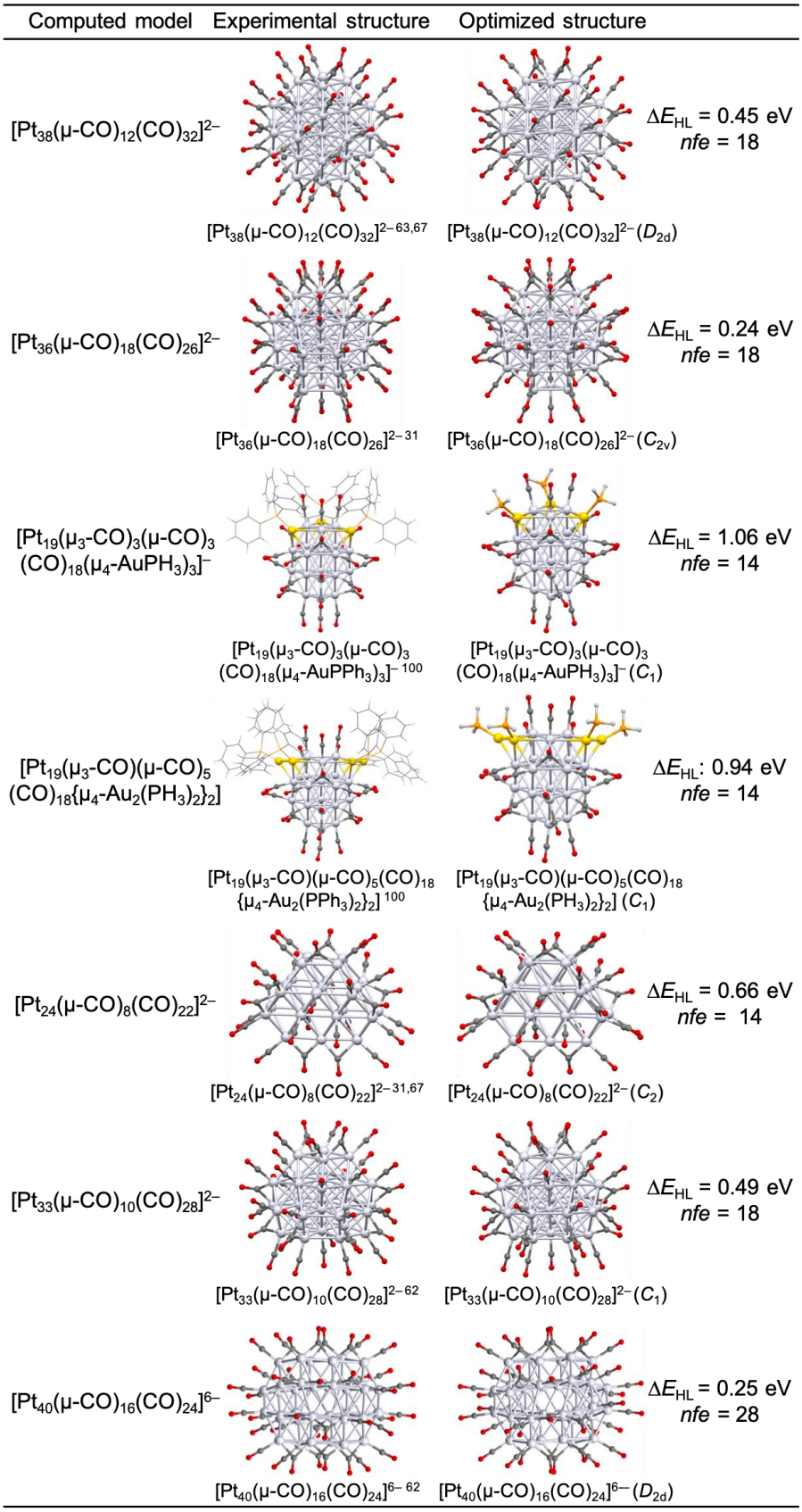

Figure 10 Optimized structures (right) of various clusters with non-spheroidal 3D architectures. ΔE_{HL} is the HOMO-LUMO gap. The corresponding experimental structures (left) are shown for comparison.

There are also clusters the shape of which cannot be derived from that of a sphere nor can be described as resulting from the condensation of smaller spherical units. Although such species cannot be rationalized within the concepts of *superatoms* or *supermolecules*, it remains nonetheless that their bonding is achieved through the population of 6s(Pt) combinations, providing their metal core remains compact enough. For example, the far from spheroidal cluster $[Pt_{24}(\mu\text{-}CO)_8(CO)_{22}]^{2-}$ [31,67] (Fig. 10, Fig. S17 and Table S19, ESI) adopts a Pt *fcc ABCA* packing of 10-, 9- and 5-atom *hc* layers. Seven orbitals with large 6s participation could be identified below the non-negligible HOMO-LUMO gap (0.66 eV), securing a 14-*fe* count. Similarly, the *fcc* core of $[Pt_{33}(\mu\text{-}CO)_{10}(CO)_{28}]^{2-}$ [62] (Fig. 10, Fig. S17 and Table S20, ESI) resulting from the packing of compact layers made of 8, 12, 9 and 4 atoms can be identified as an 18-*fe* cluster.

4. Concluding remarks

Compact platinum clusters in which the average metal configuration is $5d^{10}\ 6s^{0}$ (or very close to) cannot exist, due to their incapacity to form (enough) occupied bonding MOs with their antibonding counterparts being vacant. To compensate for this incapacity, partial average occupation of the 6s Pt AO would allow occupying strongly bonding 6s combinations. There are two ways to achieve this condition:

(i) The One is simply making highly charged anionic clusters in which the Pt atoms are in a sufficiently negative average oxidation state, such as in the experimental observed icosahedral $[Pt_{13}(CO)_{12}]^{8-}$ species ($5d^{10}\ 6s^{0.62}$).

(ii) The other way is realized by electron transfer (thus level crossing) between occupied 5d combinations and vacant 6s bonding combinations, thus achieving an "excited" $5d^{10-x}\ 6s^{x}$ average configuration. This level crossing does not occur (or is not fully completed) in the (hypothetical) bare Pt_n fragments, which are computed to be metallic (most often high-spin) systems. In fact, the level crossing is induced by the presence of the ligands which are bonded to the surface of the cluster metal core. In most of the cases, there is a terminal ligand on each of the peripheral (surface) Pt atoms, as well as additional edge- or face-bridging ligands. Whereas one may expect that *n* bridging ligands induce the destabilization of *n* 5d-type combinations, calculations showed that this is true only when *n* is small. In most of the cases the

number of destabilized 5d combinations is lower than *n*. The reason lies in the fact that the surface metal atoms use only their valence sp_σ AOs (in first approximation) for M–M and $M–CO_{terminal}$ bonding, the latter being of localized 2-center/2-electron nature. Thus, their $6p_\pi$ AOs are available for bonding with bridging ligands, in addition to the 5d ones. Anticipating the nature ($6p_\pi$ *vs.* 5d) and the respective number of the involved metal combinations is a particularly difficult task, for it depends on several individual topological parameters. In any case, the number of "supplementary" ligands is not simply related to the number of occupied 6s combinations (*nfe/2*), unfortunately. A general situation is sketched in Figure S20 (ESI), which shows the MO interaction diagram of a neutral $[Pt_n(CO)_n(\mu\text{-}CO)_m]$ species having $2m_1 < 2m$ *fe*'s.

Assuming compact ligated platinum clusters with $5d^{10-x}$ $6s^x$ average configuration, their bonding can be rationalized with the same tools as for their gold counterparts, which are of $5d^{10}$ $6s^x$ average configuration. In other words, spherical clusters can be described as *superatoms* and assemblies of spherical units as *supermolecules*. All these species have closed-shell configurations associated with *magic nfe* counts. It is however noticeable that several platinum carbonyl clusters exhibit shapes which do not allow them to be described as *superatoms*, Jahn-Teller distorted *superatoms* or *supermolecules*. In any case, the metal–metal bonding within these species is provided by the 6s orbitals. In such cases, non-spherical *jellium* models, such as for instance the *box-shaped* model,[101,102] could be useful. Observing that all the large 3D platinum clusters characterized so far have *fcc* or *hcp* metal core, a qualitative Hückel-type description of their 6s-derived electronic structure might also be useful.

Finally, it should be noted that the 5d/6s level crossing discussed above is most of the time a formally avoided level crossing. It means that substantial 5d/6s mixing occurs in the crucial bonding orbitals and pure 6s combinations do not exist. 5d orbitals also contribute to Pt–Pt bonding from the depopulation of some of their antibonding combinations. However, such a contribution does not change the number of free electrons, nor the contribution of the 6p AOs.

Author Contributions

The manuscript was written through contributions of all authors. All authors have given approval to the final version of the manuscript.

Conflicts of interest

The authors declare no competing financial interest.

Acknowledgements

The authors are grateful to GENCI (Grand Equipement National de Calcul Intensif) for HPC resources (Project A0050807367) and to the French Research National Agency (ANR-08-BLAN-0079-01) for financial support. J. W. thanks the China Scholarship Council for a Ph.D. scholarship.

Notes and references

1 H. Qian, M. Zhu, Z. Wu and R. Jin, *Acc. Chem. Res*., 2012, **45**, 1470–1479.

2 T. Tsukuda, *Springer Series in Chemical Physics (Progress in Photon Science)*, 2017, **115**, 205–218.

3 X. Kang, H. Chong and M. Zhu, *Nanoscale*, 2018, **10**, 10758–10834.

4 Q. Tang, G. Hu, V. Fung and D. Jiang, *Acc. Chem. Res*., 2018, **51**, 2793–2802.

5 Y. Pei, P. Wang, Z. Ma and L. Xiong, *Acc. Chem. Res.,* 2019, **52**, 23–33.

6 T. Higaki, Q. Li, M. Zhou, S. Zhao, Y. Li, S. Li and R. Jin, *Acc. Chem. Res.,* 2018, **51**, 2764–2773.

7 Q. Yao, T. Chen, X. Yuan and J. Xie, *Acc. Chem. Res*., 2018, **51**, 1338–1348.

8 N. A. Sakthivel and A. Dass, *Acc. Chem. Res*., 2018, **51**, 1774–1783.

9 C. M. Aikens, *Acc. Chem. Res*., 2018, **51**, 3065–3073.

10 A. Ghosh, O. F. Mohammed and O. M. Bakr, *Acc. Chem. Res*., 2018, **51**, 3094–3103.

11 S. Hossain, Y. Niihori, L. V. Nair, B. Kumar, W. Kurashige and Y. Negishi, *Acc. Chem. Res*., 2018, **51**, 3114–3124.

12 A. W. Cook and T. W. Hayton, *Acc. Chem. Res*., 2018, **51**, 2456–2464.

13 Z. Lei, X.-K. Wan, S. F. Yuan, Z.-J. Guan and Q. M. Wang, *Acc. Chem. Res*., 2018, **51**, 2465–2474.

14 S. Sharma, K. K. Chakrahari, J.-Y. Saillard and C. W. Liu, *Acc. Chem. Res*., 2018, **51**, 2475–2483.

15 K. Konishi, M. Iwasaki and Y. Shichibu, *Acc. Chem. Res.,* 2018, 51, 3125–3133.

16 J. Yan, B. K. Teo and N. Zheng, *Acc. Chem. Res*., 2018, **51**, 3084–3093.

17 C. Femoni, M. C. Iapalucci, S. Ruggieri and S. Zacchini, *Acc. Chem. Res*., 2018, **51**, 2748–2755.

18 Y. Du, H. Sheng, D. Astruc and M. Zhu, *Chem. Rev*., 2020, **120**, 526–622.

19 G. Longoni, Thesis, University of Milano, **1967**.

20 C. Femoni, M. C. Iapalucci, F. Kaswalder, G. Longoni and S. Zacchini, *Coord. Chem. Rev*., 2006, **250**, 1580–1604.

21 I. Ciabatti, C. Femoni, M. C. Iapalucci, G. Longoni and S. Zacchini, *J. Clust. Sci*., 2014, **25**, 115–146.

22 C. Cesari, J. H. Shon, S. Zacchini and L. A. Berben, *Chem. Soc. Rev.,* 2021, **50**, 9503-9539.

23 R. E. Leuchtner, A. C. Harms and Jr A. W. Castleman, *J Chem. Phys*., 1989, **91**, 2753–2754.

24 S. N. Khanna and P. Jena, *Phys. Rev. Lett*., 1992, **69**, 1664–1667.

25 S. N. Khanna and P. Jena, *Phys. Rev. B,* 1995, **51**, 13705–13716.

26 P. Jena, S. W. Khanna and B. K. Rao, *Surf. Rev. Lett*., 1996, **3**, 993–999.

27 D. E. Bergeron, P. J. Roach, Jr A. W. Castleman, N. O. Jones and S. N. Khanna, *Science,* 2005, **307**, 231–235.

28 Jr A. W. Castleman and S. N. Khanna, *J. Phys. Chem. C,* 2009, **113**, 2664–2675.

29 Z. Luo and A. W. Castleman, *Acc. Chem. Res*., 2014, **47**, 2931–2940.

30 P. Jena and Q. Sun, *Superatoms: Principles, Synthesis and Applications*, John Wiley & Sons Ltd, 2022.

31 E. Cattabriga, I. Ciabatti, C. Femoni, M. C. Iapalucci, G. Longoni and S. Zacchini, *Inorg. Chim. Acta,* 2018, **470**, 238–249.

32 D. M. P. Mingos and D. J. Wales, *Introduction to cluster chemistry*. Prentice-Hall, Englewood Cliffs, 1990.

33 F. Gam, J. Wei, S. Kahlal, J.-Y. Saillard and J.-F. Halet. *Struct. Bond.*, 2021, **188**, 69-102.

34 J.-Y. Saillard and J.-F. Halet, *Struct. Bond.,* 2016, **169**, 157−180.

35 R. D. Woods and D. S. Saxon, *Phys. Rev*., 1954, **95**, 577–578.

36 M. Walter, J. Akola, O. Lopez-Acevedo, P. D. Jadzinsky, G. Calero, C. J. Ackerson, R. L. Whetten, H. Grönbeck and H. Häkkinen, *Proc. Natl. Acad. Sci. USA,* 2008, **105**, 9157–9162.

37 H. Häkkinen, *Chem. Soc. Rev*., 2008, **37**, 1847–1859.

38 M. Zhu, C. M. Aikens, F. J. Hollander, G. C. Schatz and R. Jin, *J. Am. Chem. Soc*., 2008, **130**, 5883–5885.

39 R. S. Dhayal, J. H. Liao, Y. C. Liu, M. H. Chiang, S. Kahlal, J. -Y. Saillard and C. W. Liu, *Angew. Chem. Int. Ed*., 2015, **127**, 3773–3777.

40 R.S. Dhayal, Y. R. Lin, J. H. Liao, Y. J. Chen, Y. C. Liu, M. H. Chiang, S. Kahlal, J.-Y. Saillard and C. W. Liu, *Chem. Eur. J*., 2016, **22**, 9943–9947.

41 H. Yang, Y. Wang, J. Lei, L. Shi, X. Wu, V. Mäkinen, S. Lin, Z. Tang, J. He, H. Häkkinen, L. Zheng and N. Zheng, *J. Am. Chem. Soc*., 2013, **135**, 9568–9571.

42 M. W. Heaven, A. Dass, P. S. White, K. M. Holt and R. W. Murray, *J. Am. Chem. Soc*., 2008, **130**, 3754–3755.

43 J. Akola, M. Walter, R. L. Whetten, H. Häkkinen and H. Grönbeck, *J. Am. Chem. Soc*., 2008, **130**, 3756–3757.

44 Y. Shichibu and K. Konishi, *Small,* 2010, **6**, 1216–1220.

45 C. E. Briant, B. R. Theobald, J. W. White, L. K. Bell, D. M. P. Mingos and A. J. Welch, *J. Chem. Soc. Chem. Commun*., 1981, **5**, 201–202.

46 S. Saito and S. Ohnishi, *Phys. Rev. Lett.,* 1987, **59**, 190–193.

47 L. Cheng and J. Yang, *J. Chem. Phys*., 2013, **138**, 141101.

48 J. M. Goicoechea and S. C. Sevov, *J. Am. Chem. Soc*., 2005, **127**, 7676–7677.

49 Z. M. Sun, H. Xiao, J. Li and L. S. Wang, *J. Am. Chem. Soc*., 2007, **129**, 9560–9561.

50 I. Chakraborty and T. Pradeep, *Chem. Rev.,* 2017, **117**, 8208–8271.

51 T. H. Chiu, J. H. Liao, F. Gam, I. Chantrenne, S. Kahlal, J. -Y. Saillard and C. W. Liu, *J. Am. Chem. Soc*., 2019, **141**, 12957–12961.

52 F. Gam, C. W. Liu, S. Kahlal and J. -Y. Saillard, *Nanoscale*, 2020, **12**, 20308–20316.

53 Z. Lin, R. P. F. Kanters and D. M. P. Mingos, *Inorg. Chem*., 1991, **30**, 91–95.

54 F. K. Sheong, J. X. Zhang and Z. Lin, *Inorg. Chem*., 2016, **55**, 11348–11353.

55 M. Teramoto, K. Iwata, H, Yamaura. K. Kurashima. K. Miyazawa. Y. Kurashige, K. Yamamoto and T. Murahashi, *J. Am. Chem. Soc*., 2018, **140**, 12682–12686.

56 J. Wei, S. Kahlal, J.-F. Halet and J.-Y. Saillard, *J. Clust. Sci*., 2019, **30**, 1227–1233.

57 J. D. Erickson, E. G. Mednikov, S. A. Ivanov and L. F Dahl, *J. Am. Chem. Soc*., 2016, **138**, 1502–1505.

58 J. Wei, R. Marchal, D. Astruc, J.-Y. Saillard, J.-F. Halet and S. Kahlal, *Chem. Eur. J*., 2020, **26**, 5508–5514.

59 I. Ciabatti, C. Femoni, M. C. Iapalucci, G. Longoni, S. Zacchini and S. Zarra, *Nanoscale*, 2012, **4**, 4166–4177.

60 C. Femoni, M. C. Iapalucci, G. Longoni, S. Zacchini and S. Zarra, *J. Am. Chem. Soc*., 2011, **133**, 2406–2409.

61 F. Gao, C. Li, B. T. Heaton, S. Zacchini, S. Zarra, G. Longoni and M. Garland, *Dalton Trans.,* 2011, **40**, 5002–5008.

62 E. Cattabriga, I. Ciabatti, C. Femoni, T. Funaioli, M. C. Iapalucci and S. Zacchini, *Inorg. Chem*., 2016, **55**, 6068–6079.

63 A. Ceriotti, N. Masciocchi, P. Macchi and G. Longoni, *Angew. Chem. Int. Ed*., 1999, **38**, 3724–3727.

64 F. Fabrizi De Biani, C. Femoni, M. C. Iapalucci, G. Longoni, P. Zanello and A. Ceriotti, *Inorg. Chem*., 1999, **38**, 3721–3724.

65 A. Ceriott, F. Demartin, G. Longoni, M. Manassero, M. Marchionna, G. Piva and M. Sansoni, *Angew. Chem. Int. Ed*., 1985, **24**, 697–698.

66 S. Zacchini, *Eur. J. Inorg. Chem.,* 2011, **27**, 4125–4145.

67 J. D. Roth, G. J. Lewis, L. K. Safford, X. Jiang, L. F. Dahl and M. J. Weaver, *J. Am. Chem. Soc.,* 1992, **114**, 6159–6169.

68 D. M. Washecheck, E. J. Wucherer, L. F. Dahl, A. Ceriotti, G. Longoni, M. Manassero, M. Sansoni and P. Chini, *J. Am. Chem. Soc*., 1979, **101**, 6110–6112.

69 G. Longoni and P. Chini, *J. Am. Chem. Soc*., 1976, **98**, 7225–7231.

70 J. C. Calabrese, L. F. Dahl, P. Chini, G. Longoni and S. Martinengo, *J. Am. Chem. Soc.,* 1974, **96**, 2614–2616.

71 D. J. Underwood, R. Hoffmann, K. Tatsumi, A. Nakamura and Y. Yamamoto, *J. Am. Chem. Soc*., 1985, **107**, 5968–5980.

72 D. M. P. Mingos, *Nat. Phys. Sci.,* 1972, **236**, 99–102.

73 T. P. Fehlner, J.-F. Halet and J.-Y. Saillard, *Molecular clusters. A bridge to solid state chemistry*, Cambridge University Press, Cambridge, 2007.

74 G. Frapper and J.-F. Halet, *Rationalising and Predicting the Structure and Bonding of Bare and Ligated Transition Metal Clusters and Nanoparticles. In: Computational Materials Discovery (A. R. Oganov, A. G. Kvashnin, G. Saleh, eds.)*, Royal Society of Chemistry, London, 2019, 320−351.

75 a) G. te Velde, F. M. Bickelhaupt, S. J. A. van Gisbergen, C. F. Guerra, E. J. Baerends, J. G. Snijders and T. Ziegler, *J. Comput. Chem*., 2001, **22**, 931–967; b) ADF2018, SCM, Theoretical Chemistry, Vrije Universiteit: Amsterdam, The Netherlands, http://www.scm.com.

76 E. Van Lenthe, E. J. Baerends and J. G. Snijders, *J. Chem. Phys*., 1994, **101**, 9783–9792.

77 A. D. Becke, *Phys. Rev. A,* 1988, **38**, 3098–3100.

78 J. P. Perdew, *Phys. Rev. B,* 1986, **33**, 8822–8824.

79 S. Grimme, *J. Comput. Chem*., 2006, **27**, 1787–1799.

80 E. D. Glendening, J. K. Badenhoop, A. E. Reed, J. E. Carpenter, J. A. Bohmann, C. M. Morales and F. Weinhold, NBO 6.0, Theoretical Chemistry Institute, University of Wisconsin Madison, WI, 2001, http://nbo6.chem.wisc.edu.

81 M. J. Frisch, G. W. Trucks, H. B. Schlegel, G. E. Scuseria, M. A. Robb, J. R. Cheeseman, G. Scalmani, V. Barone, G. A. Petersson, H. Nakatsuji, X. Li, M. Caricato, A. V. Marenich, J. Bloino, B. G. Janesko, R. Gomperts, B. Mennucci, H. P. Hratchian, J. V. Ortiz, A. F. Izmaylov, J. L. Sonnenberg, D. Williams-Young, F. Ding, F. Lipparini, F. Egidi, J. Goings, B. Peng, A. Petrone, T. Henderson, D. Ranasinghe, V. G. Zakrzewski, J. Gao, N. Rega, G. Zheng, W. Liang, M. Hada, M. Ehara, K. Toyota, R. Fukuda, J. Hasegawa, M. Ishida, T. Nakajima, Y. Honda, O. Kitao, H. Nakai, T. Vreven, K. Throssell, J. A., Jr. Montgomery, J. E. Peralta, F. Ogliaro, M. J. Bearpark, J. J. Heyd, E. N. Brothers, K. N. Kudin, V. N. Staroverov, T. A. Keith, R. Kobayashi, J. Normand, K. Raghavachari, A. P. Rendell, J. C. Burant, S. S. Iyengar, J. Tomasi, M. Cossi, J. M. Millam, M. Klene, C. Adamo, R. Cammi, J. W. Ochterski, R. L. Martin, K. Morokuma, O. Farkas, J. B. Foresman and D. J. Fox, *Gaussian16*, Gaussian, Inc.: Wallingford, CT, 2016.

82 F. Weigend and R. Ahlrichs, *Phys. Chem. Chem. Phys*., 2005, **7**, 3297–3305.

83 N. de Silva and L.F. Dahl, *Inorg. Chem*., 2005, **44**, 9604–9606.

84 S. S. Kurasov, N. K. Eremenko, Y. L. Slovokhotov and Y. T. Struchkov, *J. Organomet. Chem.,* 1989, **361**, 405–408.

85 L. V. Nair, S. Hossain, S. Wakayama, S. Takagi, M. Yoshioka, J. Maekawa, A. Harasawa, B. Kumar, Y. Niihori, W. Kurashige and Y. Negishi, *J. Phys. Chem. C,* 2017, **121**, 11002–11009.

86 K. Nobusada and T. Iwasa, *J. Phys. Chem. C,* 2007, **111**, 14279–14282.

87 R. Jin, C. Liu, S. Zhao, A. Das, H. Xing, C. Gayathri, Y. Xing, N. L. Rosi, R. R. Gil and R. Jin, *ACS Nano,* 2015, **9**, 8530–8536.

88 B. K. Teo, X. Shi and H. Zhang, *J. Am. Chem. Soc*., 1991, **113**, 4329–4331.

89 B. K. Teo, H. Zhang and X. Shi, *J. Am. Chem. Soc*., 1990, **112**, 8552–8562.

90 B. K. Teo and K. Keating, *J. Am. Chem. Soc*., 1984, **106**, 2224–2226.

91 R. Hoffmann, *Angew. Chem. Int. Ed.,* 1982, **21**, 711–724.

92 D. M. P. Mingos, *Dalton Trans.,* 2015, **44**, 6680–6695.

93 H. Qian, W. T. Eckenhoff, Y. Zhu, T. Pintauer and R. Jin, *J. Am. Chem. Soc.,* 2010, **132**, 8280–8281.

94 K. Nunokawa, M. Ito, T. Sunahara, S. Onaka, T. Ozeki, H. Chiba, Y. Funahashi, H. Masuda, T. Yonezawa, H. Nishihara and M. Nakamoto, *Dalton Trans.,* 2005, **16**, 2726–2730.

95 J. S. Wright, *Can. J. Chem*., 1973, **51**, 139–146.

96 P. G. Burton and M. D. Harvey, *Nature,* 1977, **266**, 826–827.

97 L. B. Harding and W. A. Goddard III, *J. Chem. Phys*., 1977, **67**, 2377–2379.

98 B. Flemmig, P. T. Wolczanski and R. Hoffmann, *J. Am. Chem. Soc*., 2005, **127**, 1278–1285.

99 D. S. Sabirov and I. S. Shepelevich, *Comput. Theor. Chem*., 2015, **1073**, 61–66.

100 A. Ceriotti, P. Macchi, A. Sironi, S. El Afefey, M. Daghetta, S. Fedi, F. Fabrizi de Biani and R. Della Pergola, *Inorg. Chem*., 2013, **52**, 1960–1964.

101 M. J. Alhilaly, M. S. Bootharaju, C. P. Joshi, T. M. Besong, A. H. Emwas, R. Juarez-Mosqueda, S. Kaappa, S. Malola, K. Adil, A. Shkurenko, H. Häkkinen, M. Eddaoudi and O. M. Bakr, *J. Am. Chem. Soc.,* 2016, **138**, 14727–14732.

102 R. Juarez-Mosqueda, S. Kaappa, S. Malola and H. Häkkinen, *J. Phys. Chem. C,* 2017, **121**, 10698–10705.